Eur. Phys. J. B **30**, 303–312 (2002)
DOI: 10.1140/epjb/e2002-00383-6

THE EUROPEAN PHYSICAL JOURNAL B

Carrier-induced changes in the phase resolved reflection of GaAs quantum wells

Ch. Nacke, H. Stolz, G. Manzke[a], and K. Henneberger

Universität Rostock, Fachbereich Physik, 18051 Rostock, Germany

Received 29 May 2002 / Received in final form 23 September 2002
Published online 19 December 2002 –

Abstract. The influence of thermalized non-coherent carriers on the dielectric function of GaAs/AlAs quantum wells is investigated by reflection spectroscopy. Experiments are performed using the method of spectral interferometry, where both amplitude and phase of reflected pulses can be determined. For low excitation density the complex coefficient of reflection can be described using as dielectric function a broadened Elliot formula. With increasing carrier density pronounced nonlinearities appear in both amplitude and phase due to many-body effects between excited carriers. The nonlinear behavior fits very well to the results of a many-body theory based on the Semiconductor Bloch equations including memory effects in the scattering processes between carriers and the polarization induced by the probe pulse.

PACS. 71.35.-y Excitons and related phenomena – 71.45.Gm Exchange, correlation, dielectric and magnetic response functions, plasmons – 78.20.-e Optical properties of bulk materials and thin films – 78.67.De Quantum wells

1 Introduction

The nonlinear dielectric properties of semiconductor microstructures are of great interest both for device applications and from the principle point of material characterization. Addressing in this paper the influence of thermalized, incoherent carriers on the coherent dielectric response in GaAs quantum wells in the excitonic region, one has to find an accurate and convenient method to determine the response with lowest excitation density induced by the probe in a first step. In the conventional way, one measures the intensity, *i.e.* the amplitude of the reflected/transmitted beam. Then real and imaginary part of the dielectric function can be reconstructed by applying the Kramers-Kronig Relation (KKR) between them. However, the well-known problem appears, that the application of the KKR requires the knowledge of the reflection/transmission over a wide range of energy. To omit this problem and to get the full information about the investigated system, the measurement of both amplitude and phase of the test field [1–3] is necessary by *e.g.* femtosecond spectral interferometry (SI) [4,5]. By interferometry with a known reference field, the method is used to determine the complex coefficient of reflection

$$r(\omega) = |r(\omega)| \times \mathrm{e}^{\mathrm{i}\,\phi(\omega)} \tag{1}$$

measuring the phase and amplitude of reflected pulses. Due to its high sensitivity it allows to reach the regime of linear response quite easily.

In [6] SI was successfully applied to determine the refractive index and the absorption coefficient of GaAs quantum wells in dependence on the temperature. Experimental data were well described by a broadened Elliot formula, extended by KKR to the real part of the dielectric function and taking into account the confinement of carriers in the wells by a parameter of fractional dimension [7].

Studying the influence of thermalized non-coherent carriers on the optical response in quantum wells one additionally has to find appropriate methods to describe changes of the energetic position (energy shift) and the lineshape of the exciton taking the confinement of the injected carriers in the wells into account. Even though the binding energy of the exciton is increased in two-dimensional (2d) systems, many-body effects are reduced in comparison to bulk semiconductors. This was shown in [8], considering the Coulomb-Hartree Fock renormalization of excitons in the 2d case, to be the result of the confinement of carriers, which restricts the interaction between them. The influence of the screening of the Coulomb interaction on the absorption was investigated in [9], by applying a static limit for the plasmon-pole approximation of the longitudinal dielectric function. Within such a treatment, which was widely used in the literature, correlation effects in the interband selfenergy are overestimated. This results in a strong red shift of the exciton with increasing excitation (carrier density), while in the experiments the energetic position of the exciton remains nearly unchanged. Considering the sub-band quantization

[a] e-mail: manzke@physik3.uni-rostock.de

of carriers in the wells a more realistic consideration of the reduced dimensionality in quantum wells in contrast to a pure 2d-treatment was given in [10–12].

Another problem consists in an appropriate description of the increase of broadening of the exciton resonance, which was first considered by a constant dephasing rate. In order to get a better agreement with the exciton lineshape sophisticated phenomenological models for the dephasing in quantum wells were applied, describing the exponential absorption wings [13]. In [14] many-body effects were introduced phenomenologically in an Elliot formula for 2d-systems. However, in this model only selfenergy effects are considered. Since the reduction of the Coulomb interaction due to phase-space filling and screening is not taken into account the exciton experiences a large red shift, which is still larger than that in the treatments [9,10].

A strict microscopic consideration of many-body effects based on the Semiconductor Bloch Equations (SBE) [15] was presented in [16,17]. Here the many-body effects arise *via* scattering terms in the kinetic equations for the coupled two-band density matrix. This scattering terms can be split into two classes, describing so-called diagonal (selfenergy) and off-diagonal correlation effects (reduction of the Coulomb interaction), which both compensate one another. While the interplay of the real parts leads to a nearly unchanged position of the exciton resonance, the off-diagonal dephasing compensates partially the diagonal dephasing and results in a correct description of the gain at lower energies [18].

An additional aspect came into the discussion by investigating memory effects in the scattering terms (quantum-kinetic description) [19,20]. Meanwhile, unambiguous signatures of quantum-kinetic effects were found for both electron-LO-phonon and electron-electron scattering (see [21–23] and papers cited there). For bulk GaAs we have demonstrated in [24] that memory effects in the scattering terms play an important role for the linear optical response. Considering a thermal population of carriers the solution of the SBE's can be simplified by Fourier transformation, where the memory effects result in a dependence of the many-body effects on the energy of the exciting test pulse. The energy dependence is responsible for the correct description of the spectral properties (shift and lineshape) and of the behavior of the phase of transmitted pulses.

Our experimental setup is characterized in Section 2. In Section 3 we start with the investigation of the optical response of the non-excited sample, in order to fit the exciton parameters, and develop a convenient theoretical model for the dielectric function in the wells. We will show, that as in [6] our results fit very well with a broadened Elliot formula for systems with broken dimension, extended by the corresponding real part *via* KKR [7]. Here the reduced dimensionality in the wells is fitted by a parameter getting best agreement with the experiment. We also solve the SBE's considering the confinement of carriers by an expansion with respect to the sub-band-wave functions in the wells. We get perfect agreement of the real and imaginary part of the dielectric function with the result from the broadened Elliot formula. This allows us to investigate

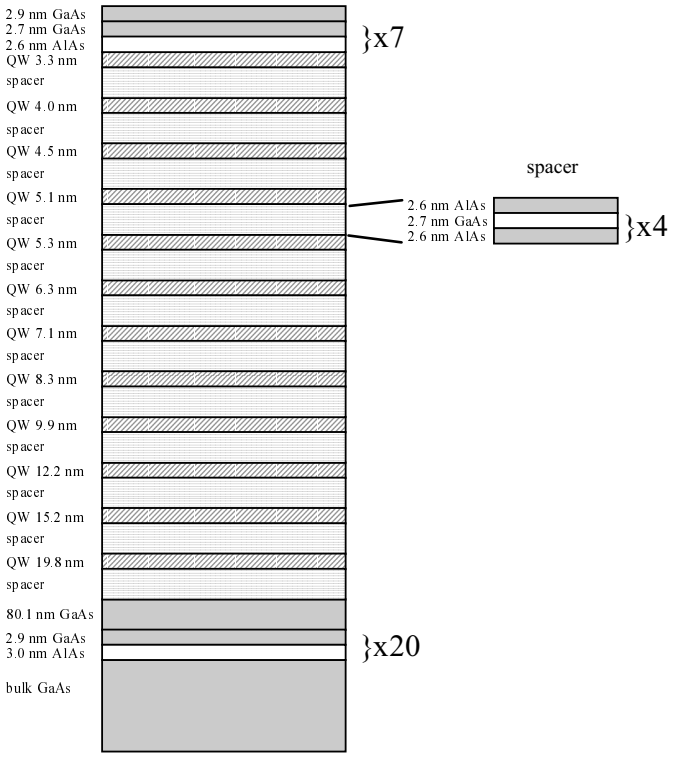

Fig. 1. Sample structure.

the influence of thermalized non-coherent carriers in Section 4 on the linear optical response including the many-body effects between carriers and the laser-induced polarization in the SBE's. We extend our many-body approach presented in [24] for bulk semiconductors to quantum wells, where in contrast to earlier treatments quantum kinetic effects are considered. We show, that the results of our many-body approach agree with the experimental findings.

2 Experiment

The investigated sample (see Fig. 1) is a high quality quantum well structure grown by molecular-beam epitaxy on a GaAs substrate [25] and contains a series of single quantum wells with l_Z from 3.3 nm up to 83 nm separated by AlAs/GaAs superlattices, where only those with well width l_Z ranging from 9.9 nm up to 19.8 nm were studied in detail.

To perform SI we use a stabilized Mach-Zehnder interferometer (Fig. 2, top) with a piezo-actuator controlled by a capacitive sensor element inside a PID servo loop. The accuracy of the interferometer as tested by a HeNe laser autocorrelation measurement is about 0.022 fs. SI requires a reference field with a well known phase. Therefore the chirp of a 120 fs titan-sapphire laser pulse is carefully minimized by a prism pulse compressor and controlled using a SHG-FROG setup [2,26].

This chirp free pulse is divided into two replicas using a beam splitter. One beam is focused on the quantum

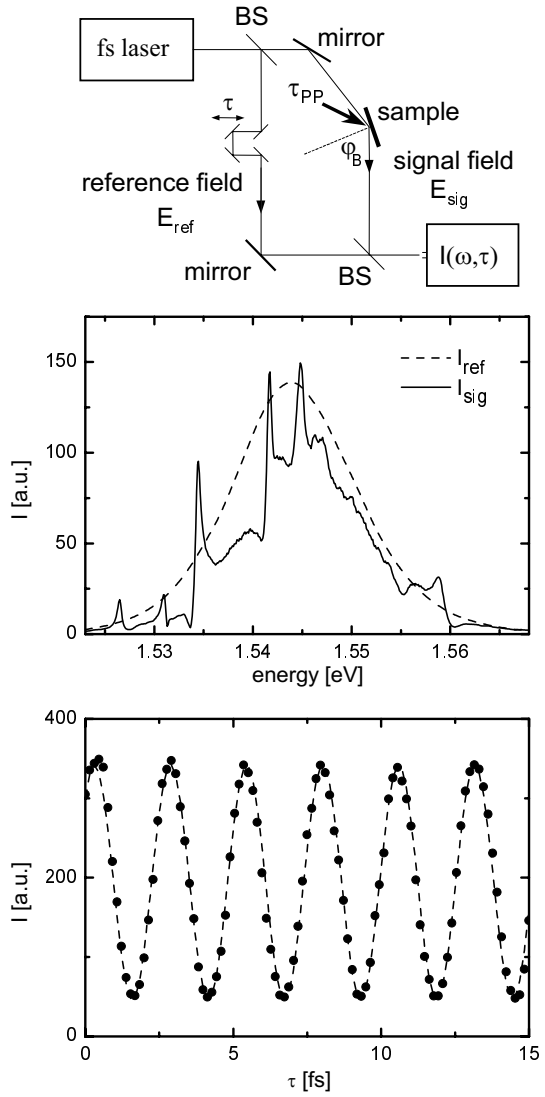

Fig. 2. Experimental setup (top), reference and signal spectra (middle), temporal interferogram for fixed frequency ($\hbar\omega$ = 1.5412 eV, bottom).

well sample and the reflex is called signal field $E_{\rm sig}$. The other beam is used as the time delayed reference field $E_{\rm ref}$, mode-matched and collinearly recombined with the signal field using a second beam splitter and send to a CCD spectrometer with a resolution of 0.4 meV.

The sample is mounted on a copper block in a He flow cryostat and was held at $T = 12$ K. The probe beam is focused to a spot size of 40×70 μm^2, the pump beam to a size of 70×150 μm^2. The pump beam arrives non-collinearly to the probe and at fixed delay time $\tau_{PP} = 20$ ps before the probe.

The strong non-resonant reflection due to the background index of reflection was efficiently suppressed by measuring the reflected laser pulse for incidence at the Brewster angle ($\phi_B = 72°$).

The measured spectral interferogram $I(\omega, \tau)$ is given as a Fourier transformed superposition of reference $E_{\rm ref}$ and signal field $E_{\rm sig}$ in time domain:

$$\begin{aligned} I(\omega,\tau) &= \left| \int_{-\infty}^{\infty} {\rm d}t \, (E_{\rm ref}(t-\tau) + E_{\rm sig}(t)) {\rm e}^{{\rm i}\omega t} \right|^2 \qquad (2) \\ &= I_{\rm ref}(\omega) + I_{\rm sig}(\omega) \\ &+ 2\,|E_{\rm ref}(\omega)|\,|E_{\rm sig}(\omega)| \cos(\phi_{\rm sig}(\omega) - \phi_{\rm ref}(\omega) - \omega\tau). \end{aligned}$$

According to equation (2) we first record the reference and signal spectra by blocking one beam (Fig. 2, middle) and then the interferogram for several time delays.

There are in principle two ways to analyze such interferograms. The first is the Fourier transform spectroscopy [4], which consists of Fourier transforming the data into the time domain where two mirror images of the temporal dependence exist. The negative time curve can be neglected and an inverse Fourier transformation gives the full complex field in frequency domain. We preferred another way by changing the time delay interferometrically controlled, so that *e.g.* the stability of the interferometric setup is obvious. For a fixed frequency ω the measured data can be fitted by cosine function (Fig. 2, bottom):

$$I(\omega,\tau) = A(\omega) + B(\omega)\cos(C(\omega) - \omega\tau). \qquad (3)$$

The signal field can be evaluated with the measured chirp free reference field ($|E_{\rm ref}(\omega)| = \sqrt{I_{\rm ref}(\omega)}$, $\phi_{\rm ref}(\omega) = 0$) by a comparison of coefficients between equations (2) and (3):

$$E_{\rm sig}(\omega) = |E_{\rm sig}(\omega)|{\rm e}^{{\rm i}\phi_{\rm sig}(\omega)} \qquad (4)$$

$$= \frac{B(\omega)}{|E_{\rm ref}(\omega)|}{\rm e}^{{\rm i}\,C(\omega)}. \qquad (5)$$

3 Linear properties

In the case of weak probe pulses (linear response), the reflected signal field can be written as

$$E_{\rm sig}(\omega) = r(\omega) E_{\rm ref}(\omega) \qquad (6)$$

and the complex coefficient of reflection can be easily estimated for a chirp free reference field.

The measured complex coefficient of reflection at low temperature ($T = 12$ K) and at low excitation fluences $F_0 = 0.6$ nJ/cm^{-2} without the pump pulse is shown in Figure 3 (solid line). The exciton resonances for the quantum wells are clearly separated and can be assigned to the heavy and light hole excitons in the single wells. The carrier density induced by the test pulse, which can be estimated using the absorption of the quantum well (Fig. 4), is about $n = 2.1 \times 10^7$ cm^{-2}, and low enough to be in regime of linear response. We find pronounced changes of the phase at the single exciton resonances, which differ from well to well, showing a jump-like or a more dispersive behavior. In order to describe the behavior of the complex coefficient of reflection in Figure 3 we have calculated the light propagation through the sample using a many-layer model and standard matrix techniques, which takes into account the non-resonant and the excitonic parts of the

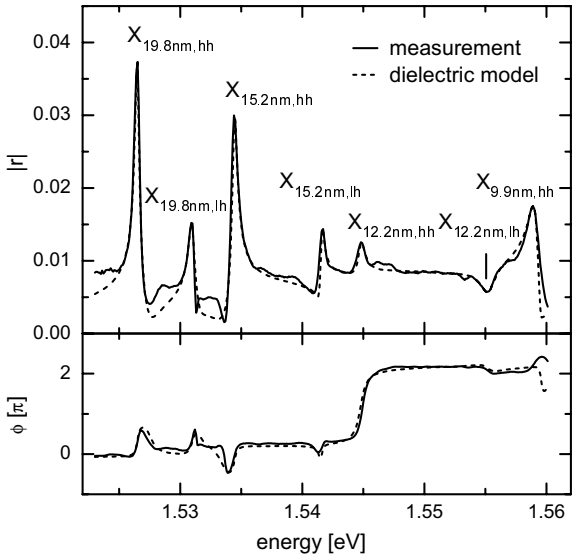

Fig. 3. Complex coefficient of reflection: measurement (solid line) and dielectric model (dashed).

dielectric function of the superlattices and quantum wells, respectively. We assumed a local susceptibility for each well, since the width is much smaller then the wave length.

The dielectric properties of the superlattice are specified by the dielectric properties of GaAs and AlAs without any excitonic effects. The background dielectric function $\varepsilon_B(\omega)$ is given by a single effective oscillator [27]:

$$\varepsilon_B(\omega) = 1 + \frac{E_d}{E_0}\,\frac{1}{1-(\hbar\omega/E_0)^2}\,. \tag{7}$$

We use for GaAs (AlAs) the oscillator strength $E_d = 32\,(33.65)$ and the energy $E_0 = 3.74$ eV (4.8 eV). Due to the superlattices acting as barriers between the wells the total number of layers in the sample is 177. In order to simplify the calculations effective dielectric functions for the superlattices are introduced

$$\varepsilon_{\mathsf{eff}}(\omega) = \frac{\sum_i l_Z^i \varepsilon_B^i(\omega)}{\sum_i l_Z^i}\,. \tag{8}$$

Consequently our effective model is composed of 14 layers including five GaAs quantum wells (9.9 nm to 83 nm).

The dielectric function of the wells is composed of three components: the part of (i) the heavy and (ii) light hole exciton described by a broadened Elliot formula within the Tanguy-model [7] and (iii) the background part. The exciton resonance is described by the oscillator linewidth (damping) γ, the strength A and the parameter of the effective dimension d in regard to the finite quantum confinement [5]. Moreover we use an energy dependent damping $\gamma(\omega)$ according to [24]

$$\gamma(\omega) = \gamma_0\, f(\omega)\,,\; f(\omega) = c_1 + c_2\,\tanh\left(c_3\,\omega + c_4\right), \tag{9}$$

which reduces the influence of the higher excited exciton states ($2s$, $3s$,...) in the region from the $1s$-exciton to the band gap by a higher damping. The parameters $c_1, \ldots, c_4$ are chosen as follows: damping of the $1s$-state is taken to be $\gamma(E_{gap}-E_{ex}^{b,d}) = \gamma_0$, with $E_{ex}^{b,d}$ being the binding energy of the $1s$-exciton in the quantum well, the damping of the $2s$-state $\gamma(\omega_{2s}) = 5\,\gamma_0$, as the limit high in the band $\gamma(\omega \gg E_{gap}) = 6\,\gamma_0$ (E_{gap} - gap energy) is set, and the asymptotic $\gamma(\omega \ll E_{gap}-E_{ex}^{b}) = 0.5\,\gamma_0$ is fitted to get best agreement with the experiment. This damping is introduced more or less phenomenological, taking into account the influence of phonons and impurities, and leads to better agreement of the theoretical model with the experimental findings for the non-excited sample.

Table 1. Fit parameters for complex coefficient of reflection within the Tanguy model.

l_Z/nm	d	A_{hh}/eV$^{3-\frac{d}{2}}$	γ_{hh}/meV	A_{lh}/eV$^{3-\frac{d}{2}}$	γ_{lh}/meV
19.8	2.53	0.12	0.16	0.09	0.26
15.2	2.46	0.10	0.19	0.04	0.14
12.2	2.40	0.13	0.30	0.10	0.96
9.9	2.36	0.17	0.45	-/-	-/-

The exciton parameters for the single wells are determined to give the best fit to the experiment. The resulting complex coefficient of reflection is presented in Figure 3 by the dashed line, the exciton parameters are given in Table 1. We find an excellent agreement both in amplitude and in phase between the measured and the modeled coefficient of reflection over the whole spectral range.

Alternatively, we have calculated the susceptibility $\chi(\omega)$ for the different quantum wells by solving the semiconductor Bloch equations (SBE) for the laser induced polarization $p_k(\omega)$

$$\left\{\omega - k^2 + \mathrm{i}\gamma(\omega)\right\}\, p_k(\omega) + \sum_q\, \tilde{v}_{k-q}^{eh}\, p_q(\omega) = d_{cv}\, E(\omega), \tag{10}$$

where d_{cv} is the dipole matrix element, and E the electric field. We have used the energy dependent damping (9), taking into account the increase of damping towards to the band gap. The damping constant γ_0 is fitted to the linewidth of the exciton ($1s$-state) taken from the experiment at lowest excitation. The Coulomb interaction $\tilde{v}_q^{eh}$ is used in quantum well representation [10–12,16]:

$$\tilde{v}_q^{eh} = \frac{4\pi}{q}\, J_q^{eh}, \tag{11}$$

$$J_q^{eh} = \int \mathrm{d}z_e\, \mathrm{d}z_h\, |\Phi_e(z_e)|^2\, |\Phi_h(z_h)|^2 \mathrm{e}^{-q(z_e-z_h)}. \tag{12}$$

Here the function J_q^{eh} describes the deviation of the quasi-2d quantum well potential $\tilde{v}_q^{eh}$ from the pure 2d-Coulomb interaction $v_q^{2d} = 4\pi/q$ (we use 3D-exciton parameters throughout the paper). In comparison to the bulk case the SBE is reduced to an effective two-dimensional description with the two-dimensional wave vector q in the plane perpendicular to the growth direction of the sample. The confinement in growth direction is accounted by the eigenfunctions $\Phi_a(z_a)$ of electrons/holes (a=e, h) in the quantum well.

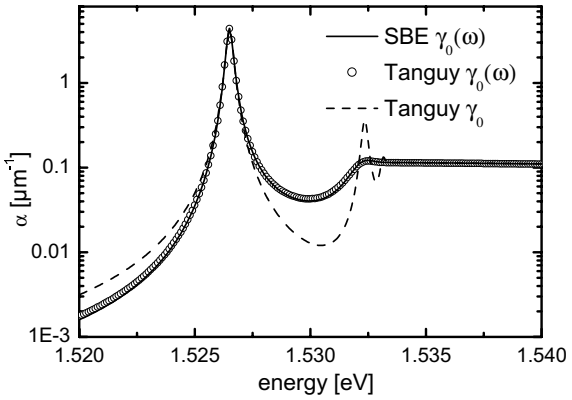

Fig. 4. Comparison of calculated absorption coefficients of the 19.8 nm quantum well: Broadened Elliot formula (Tanguy [7]) and SBE (10).

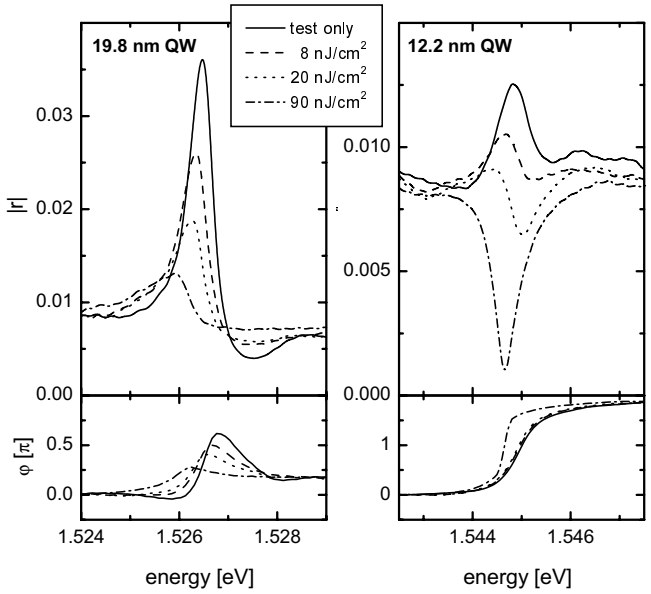

Fig. 5. Experimental complex coefficient of reflection: 19.8 nm and 12.2 nm quantum well, dependence on pump fluence.

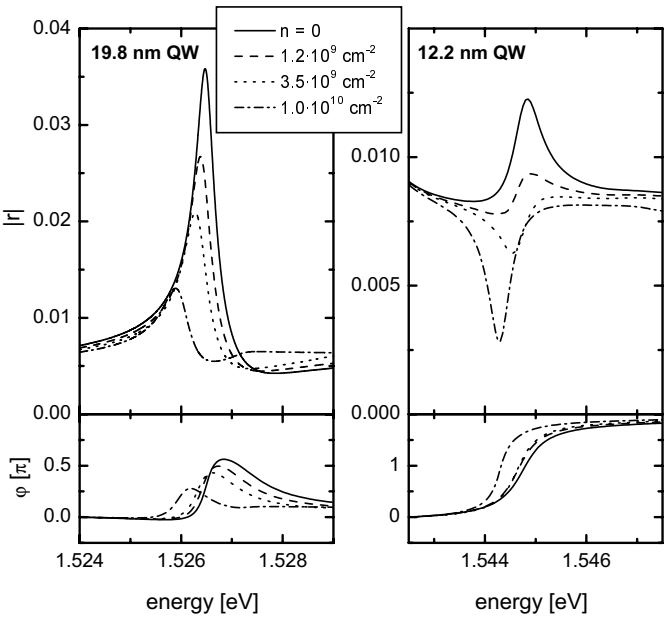

Fig. 6. Theoretical complex coefficient of reflection: 19.8 nm and 12.2 nm quantum well, dependence on carrier density. This figure will be discussed at the end of the paper.

In order to simplify our representation we have dropped the quantum numbers of the single sub-band levels and considered only the ground states. For the investigated quantum wells with well width not larger than 20 nm this limitation is valid since the separation of the sub-band energies is large enough. Moreover, coupling between single sub-bands is neglected. In a complete quantum-well representation the quantum-well interaction (11) would depend on four sub-band levels and the polarization on two, correspondingly. However, within our approximation we are able to explain all features found in the experiment. Moreover we find excellent agreement for the imaginary part of the susceptibility between the microscopic approach (10,11) and the phenomenological treatment of the reduced dimensionality with the broadened Elliot formula [7] (Fig. 4). The deviations are below 1%. For comparison the result with a constant damping (fixed at the 1s-exciton resonance) is given, where the 2s-exciton would be clearly resolved. However, this is in contrast to the experimental findings presented in Figure 3, where the higher exciton states are damped out.

In our microscopic approach the position of the exciton resonances in the single wells results from the quantum confinement of the carriers and the binding energy $E_{ex}^{b,d}$ due to the quasi-two dimensional Coulomb interaction (11). As the only parameters we have adjusted the band offset between the GaAs wells and the AlAs/GaAs superlattices, separating the wells, and the effective masses of carriers in the superlattices. The phenomenological parameter of the effective dimensionality d in Table 1 is connected with the exciton binding energy (1s-state) *via* $E_{ex}^{b,d} = 4\,E_{ex}^{b}/(d-1)^2$.

The good agreement of our microscopic approach with the experiment is the pivotal presupposition to extend the SBE (10) in Section 4 by many-body effects between excited carriers, in order to investigate the dielectric functions, as well as phase and amplitude of reflected fields for the case of pre-pumped samples. We stay on a strict microscopic level and omit any phenomenological introduction of renormalized energies and models for an increasing damping of the exciton resonances into the broadened Elliot formula, which compulsorily fails (see discussion in Sect. 4).

For the non-excited sample the complex dielectric functions in the wells are fixed by the broadened Elliot formula with the parameters given in Table 1. If the susceptibility is calculated *via* SBE's one has the well-known problem, to determine the real part *via* KKR from the imaginary part. This problem vanishes, if the KKR of

the difference between the imaginary parts of the susceptibility for the excited and the non-excited sample is performed, since the carrier-induced changes are limited around the exciton resonance up to the band gap.

4 Nonlinear properties

In this section the nonlinear properties of phase and amplitude of reflected fields are investigated, which arise due to many-body effects between incoherent, thermalized carriers generated by non-collinear pump pulses of different intensity. The pump pulse arrives the sample 20 ps before the probe, so that scattering processes destroy the macroscopic polarization induced by the pump before the probe pulse arrives.

The pump-induced modifications of the reflection coefficient are shown in Figure 5 for different fluences and two wells (19.8 nm, 12.2 nm). We find pronounced changes of both amplitude and phase in the vicinity of the excitons in all the wells. The changes in the amplitude with increasing excitation are similar in all wells. The excitonic features are broadened and smeared out and undergo a small red shift. Concerning the phase the changes differ from well to well. In the 19.8 nm well with a more dispersive behavior of the phase and a bump around the resonance and only a small jump for the unexcited sample, the changes of the phase with increasing excitation are similar to those of the amplitudes. A different behavior is observed for the phase in the 12.2 nm well: Here the jump of the phase by nearly 2π becomes still more pronounced with increasing excitation.

Theoretical calculations point out that delicate features of the complex coefficient of reflection yield a finger-print of the spatial and dielectric properties of the investigated sample, *e.g.* small changes in the sample structure lead to significant changes in the phase spectrum. Nevertheless a physical interpretation of the behavior of the spectral phase is difficult. A similar effect was found in [24] investigating the temporal evolution of transmitted pulses in bulk GaAs. There a change of the sign of jumps of the temporal resolved phase from $+\pi$ to $-\pi$ was observed at polariton beats. A more detailed analysis has shown, that the jumps become nearly step-like near that excitation intensity, where the jumps change their sign. This could be explained by interferences of the different polariton waves propagating through the sample, which are sensitively against changes of the group velocity induced by many-body effects between carriers. So we deduce, that the different behavior of the phases of both wells in the non-excited case results from the changes of these interferences due the different locations of the wells in the sample.

In order to give a theoretical explanation of the behavior of the reflected light with increasing excitation we extend the SBE (10) by inclusion of many-body effects between excited carriers. Therefore we extend the treatment in [24] developed for bulk materials to quantum wells. We don't repeat all the steps of the derivation in [19], since this describes the Fourier transformation of the time dependence in the quantum kinetic scattering terms into energy dependent many-body effects, being independent on the confinement of the carriers in the wells. For a more detailed presentation we refer to our theoretical investigations in [30]. The structure of the SBE remains unchanged.

$$\left\{\omega - k^2 - \Delta_k^{HF} + \mathrm{i}\gamma(\omega) - \Sigma_k^r(\omega)\right\}\, p_k(\omega) + \sum_q \left\{N_k\, \tilde{v}_{k-q} + \Theta_{k,q}(\omega)\right\}\, p_q(\omega) = N_k\, d_{cv}\, E(\omega). \quad (13)$$

As consequence of screening the Coulomb interaction between carriers will be renormalized by the effective interaction $\Theta_{k,q}(\omega)$, the Coulomb-HF energy Δ_k^{HF} and the retarded interband selfenergy $\Sigma_k^r(\omega)$ describing the renormalization of the interband energy and the dephasing. The interband selfenergy arises from collisions between carriers, the effective interaction from collisions between carriers and the laser-induced polarization. The Pauli-blocking factor $N(k) = 1 - f_k^e - f_k^h$ accounts the phase space occupation for fermions, $f_a(k)$ are the distribution functions for electrons/holes. For vanishing excitation ($f^a \to 0$) equation (13) turns into (10). Since the delay between pump and probe pulse is large enough the carriers can be considered to be in quasi-equilibrium and both distributions are taken as Fermi functions. As in (10) sub-band levels for the confined electrons and holes in the well are dropped and only the lowest state is considered.

The structure of the effective interaction matrix corresponds to that in bulk case

$$\Theta_{k,q}^{ab}(\omega) = \sum_{a\neq b} \int \frac{\mathrm{d}\bar{\omega}}{2\pi}\, \frac{[1 - f_k^a]\tilde{V}_{k-q}^{ab,>}(\bar{\omega}) + f_k^a\, V_{k-q}^{ab,<}(\bar{\omega})}{\omega - \varepsilon_k^a - \varepsilon_q^b - \bar{\omega} + \mathrm{i}[\Gamma_k^a + \Gamma_q^b]/2}. \quad (14)$$

We use the same notation as in [24], where $\varepsilon_k^a = e_k^a - \Delta_k^{a,HF} - \mathrm{Re}\,\Sigma_{aa,k}^r(\varepsilon_k^a)$ describes the renormalization of the carrier energy e_k^a and $\Gamma_k^a = -2\,\mathrm{Im}\,\Sigma_{aa,k}^r(\varepsilon_k^a)$ the damping of carrier states in quasi-particle approximation (QPA). Both are connected with the retarded carrier selfenergy

$$\Sigma_{aa,k}^r(\varepsilon_k^a) = \sum_q \int \frac{\mathrm{d}\omega}{2\pi}\, \frac{[1 - f_q^a]\, \tilde{V}_{k-q}^{aa,>}(\omega) + f_q^a\, \tilde{V}_{k-q}^{aa,<}(\omega)}{\varepsilon_k^a - \varepsilon_q^a - \omega + \mathrm{i}\Gamma_q^a/2}. \quad (15)$$

The Hartree-Fock energy is given by $\Delta_k^{a,HF} = \sum_q \tilde{v}_{k-q}^{aa}\, f_q^a$. Equation (15) describes the influence of many-body effects on the one-particle properties of carriers $(\varepsilon_k^a, \Gamma_k^a)$ and has to be solved by iteration (see the discussion in [24]). The interband selfenergy

$$\Sigma_k^r(\omega) = \sum_{a\neq b} \sum_q \int \frac{\mathrm{d}\bar{\omega}\, [1 - f_q^b]\tilde{V}_{k-q}^{aa,>}(\bar{\omega}) + f_q^b\, \tilde{V}_{k-q}^{aa,<}(\bar{\omega})}{2\pi\ \ \omega - \varepsilon_k^a - \varepsilon_q^b - \bar{\omega} + \mathrm{i}[\Gamma_k^a + \Gamma_q^b]/2} \quad (16)$$

depends on the energy ω of the photon, which generates an electron-hole pair under absorption/emission of a plasmon. In the bulk case there is a simple relation between interband selfenergy and the effective interaction $\Sigma_k^r(\omega) = \sum_q \Theta_{q,k}(\omega)$. This is not valid in the quantum

well case considered here. Due to the different confinement of electrons and holes in the wells V depends on the carrier species $a, b = e, h$. Within RPA (Random Phase Approximation) it is given by

$$\tilde{V}_q^{ab,>/<}(\omega) = \sum_c \tilde{V}_q^{ac,r}(\omega)\, P_q^{cc,>/<}(\omega) \tilde{V}_q^{cb,r}(\omega), \quad (17)$$

where the retarded screened interaction is used in a static approximation

$$\tilde{V}_q^{ab,r}(\omega) \longrightarrow \frac{4\pi}{\sqrt{q^2+\kappa^2}}\, J^{ab}_{\sqrt{q^2+\kappa^2}} = \tilde{v}^{ab}_{\sqrt{q^2+\kappa^2}}. \quad (18)$$

Here in contrast to the bare quantum-well interaction (11) the wave number q has to be replaced by $\sqrt{q^2+\kappa^2}$. The longitudinal polarization $P^{>/<}$ is used in RPA and calculated using its relation to the imaginary part of the retarded polarization

$$P_q^{aa,>/<}(\omega) = n^{>/<}(\omega)\, \mathrm{Im} P_q^{aa,r}(\omega) \quad (19)$$

$$\mathrm{Im} P_q^{aa,r}(\omega) = \int \frac{\mathrm{d}^2 k}{2\pi} \left[f_k^a - f_{k-q}^a \right] \delta(\omega - e_{k-q}^a + e_k^a), \quad (20)$$

where $n^{>}(\omega) = 1 + n^{<}(\omega)$, and $n^{<}(\omega)$ is a Bose function. Equation (19) corresponds to a 2-dimensional limit of the Lindhard formula.

We still haven't considered the complete dynamical screening for the 2d-case due to its numerical effort. Using the static approximation for the retarded screened potential (18), we neglect the spectral properties of plasmons and replace it by its value at $\omega = 0$. Otherwise, for low carrier densities the polarization $P^{>/<}$ is strongly located at small ω, which cuts the influence of spectral properties of plasmons. Finally, we have considered the main influence of the dynamical character of screening stemming for lower carrier densities from the dynamical polarization $P^{>/<}$. For the bulk case we have checked numerically, that complete dynamical screening becomes important for higher carrier densities, *e.g.* in the vicinity of the Mott transition of the exciton and above, where gain appears [28]. The treatment above has already been used in the literature to describe the basic excitonic and gain properties in ZnSe [16].

Furthermore we find, that the consideration of the different confinement of electrons and holes leading to different interaction potentials $\tilde{v}^{ee}, \tilde{v}^{hh}, \tilde{v}^{eh}$ has only a minor influence on the effective interaction (14) and the interband selfenergy (16). Replacing all interactions by $\tilde{v}^{eh}$ has proved to be a good approximation, which reduces the numerical effort considerably, and can be understood as result of the summations over the species (e, h) in (14–17). These properties are important for the behavior of the shift of the exciton resonance with increasing excitation. For the bulk case we have demonstrated [24,29], that a strong compensation appears between the selfenergy (16) and the effective interaction (14), which results in a nearly unchanged position of the exciton, being in accordance with the experiment. As we will demonstrate in the following, this is also valid for the quantum-well case with its reduced dimensionality. On the other hand this compensation prevents the possibility of a simple extension of the broadened Elliot formula considering the selfenergies of carriers without taking into account the many-body renormalization of the bare Coulomb interaction by the effective interaction.

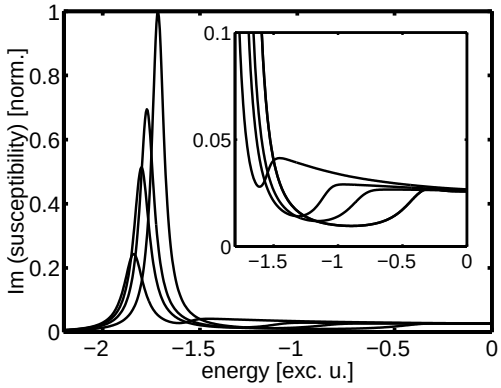

Fig. 7. Imaginary part of the susceptibility of a 19.8 nm GaAs-GaAlAs quantum well at a carrier temperature of 20 K and for different carrier densities ranging from above to below: $n = 0, 1.2\times10^9$ cm^{-2}, 3.5×10^9 cm^{-2}, 1.0×10^{10} cm^{-2}. The shift of the band gap is demonstrated in the inset.

We have solved equation (13) for the coherent polarization including many-body effects as describe above. The imaginary part of the susceptibility $\chi(\omega) = \sum_k p_k(\omega)/E(\omega)$ (absorption) is shown in Figure 7 for different carrier densities. The energy is given in excitonic units $(E - E_g)/E_{ex}^b$ with the gap energy E_g and the binding energy $E_{ex}^b = 4.2$ meV for bulk GaAs.

With increasing carrier density the exciton resonance becomes more and more broadened with a small red shift. The band gap shifts downward to the exciton (see inset). The Mott transition appears slightly above $n = 1.0\times10^{10}$ cm^{-2}.

In order to demonstrate the role of quantum-kinetic effects, which are reflected in the dependence of interband selfenergy (16) and interaction matrix (14) on the energy, we compare our results with those of a Markovian approximation of scattering terms in SBE's. In this case both many-body quantities don't depend on the energy, *e.g.* the interband selfenergy looks similar like the sum of the quasi-particle selfenergies (15) for electrons and holes:

$$\Sigma_k^{r,QPA} = \sum_a \sum_q \int \frac{\mathrm{d}\bar{\omega}}{2\pi} \frac{[1-f_q^a]\tilde{V}_{k-q}^{aa,>}(\bar{\omega}) + f_q^a\, \tilde{V}_{k-q}^{aa,<}(\bar{\omega})}{\varepsilon_k^a - \varepsilon_q^a - \bar{\omega} + \mathrm{i}[\Gamma_k^a + \Gamma_q^a]/2}. \quad (21)$$

The imaginary part of this interband selfenergy was earlier used as an approximation for the dephasing rate [31]. A more physical understanding of results within the quantum-kinetic and Markovian approximation is received, comparing the denominators in (16) and (21). The denominator in the quantum-kinetic case becomes resonant for $\omega = \varepsilon_k^a + \varepsilon_q^b + \bar{\omega}$, describing the excitation of an electron-hole pair of the energy $\varepsilon_k^a + \varepsilon_q^b$ by the probe pulse photon of energy ω, accompanied by absorption/emission

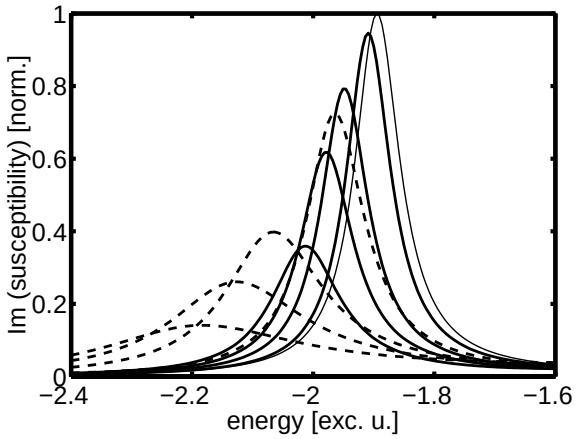

Fig. 8. Imaginary part of the susceptibility of a 15.2 nm GaAs-GaAlAs quantum well at a carrier temperature of 20 K and for different carrier densities ranging from above to below: $n = 0$ (thin line), 7.5×10^8 cm^{-2}, 1.2×10^9 cm^{-2}, 3.5×10^9 cm^{-2}, 1.0×10^{10} cm^{-2}, quantum kinetics (solid lines), Markovian approximation (dashed lines).

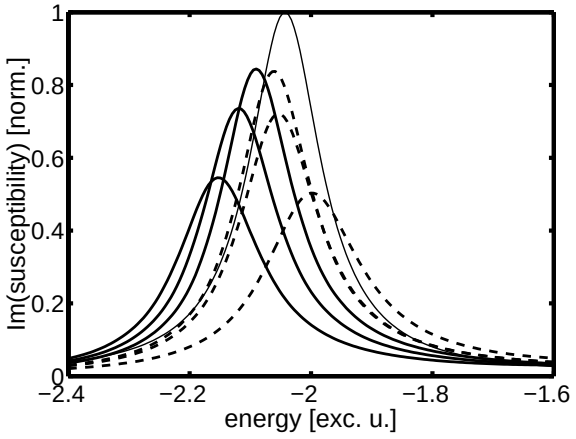

Fig. 9. Imaginary part of the susceptibility of a 12.2 nm GaAs-GaAlAs quantum well at a carrier temperature of 20 K (thick solid lines), 10 K (dashed) and for different carrier densities ranging from above to below: $n = 0$ (thin line), 1.2×10^9 cm^{-2}, 3.5×10^9 cm^{-2}, 1.0×10^{10} cm^{-2}.

of a quantum $\bar{\omega}$ of the longitudinal elementary excitations in the e-h plasma. In the Markovian case an intraband transition similar to that in a Boltzmann scattering term appears, which has nothing do to with an interband transition. This is a further general argument for the validity of the quantum-kinetic approach. A quantitative comparison of both approaches is presented in Figure 8. The differences are obvious, within the Markovian treatment the exciton is much more broadened and shifted. This is the direct consequence of the dependence of many-body effects on the energy. For $k = 0$ and $\omega = 0$ (at the band edge) both expressions for the interband selfenergy (16) and (21) become identical. However, while *e.g.* the diagonal dephasing within the quantum-kinetic approach is peaked at the band edge and decreases towards the exciton and higher energies, the constant value of dephasing rate in the Markovian approximation is used over the whole energy range. Thus, a much larger value for the dephasing is used in the Markovian approximation. The same holds for the off-diagonal dephasing and the corresponding real parts of the interband selfenergy and the effective interaction. The latter explains the stronger shift of the exciton within Markovian approximation. Finally, one can state from the viewpoint of the theory, although a Markovian approximation simplifies the scattering terms in the SBE's in comparison to that of a quantum kinetic treatment, it is not valid to describe the properties of the linear optical response in quantum wells at low temperatures. We have checked numerically, that at room temperature the deviations of the susceptibility between both approaches become weaker. This is due to the weaker decrease of the dephasing and the interband energy from the band edge towards the exciton.

The dependence of the exciton shift on the temperature is demonstrated in Figure 9 for the 12.2 nm GaAs-GaAlAs quantum well. For 10 K the position of the exciton starts to shift with increasing density to higher energies (blue shift), while it turns to red for higher temperatures. This behavior is typical for all wells. Generally the shift of the exciton resonance arises from the interplay of the reduction of the band gap (HF-shift and real part of the interband selfenergy (16)) and the reduction of the Coulomb interaction due to the effective interaction (14). The resulting dependence on the temperature is similar as observed in the bulk case for ZnSe around 30 K [29]. There it could be explained by the dominant Pauli blocking N_k, reducing the interaction strength at lower temperatures.

We don't know the exact temperature of carriers in the single wells for the different excitation intensities and use the temperature as a parameter in order to fit the shift of the exciton for the different carrier densities according to the measured reflection. Since our sample (see Fig. 1) consists of a series of single quantum wells the total absorption in the wells is small and the excitation is considered to be constant in all the wells. The propagating probe light is finally absorbed in the GaAs buffer. The final results for the complex coefficient of reflection are presented in Figure 6, which is placed above for better comparison with the experiment Figure 5. The theoretical result shows all characteristic changes observed in the experiment, demonstrating the validity of the approach. Most important, the carrier densities estimated from the experiment agree well with the densities in the theoretical description, *e.g.* the highest fluence in Figure 5 corresponds to $n = 0.7 \times 10^{10}$ cm^{-2} [32]. This agreement with the experiment cannot be achieved using the results of a Markovian approximation for the scattering terms in the SBE's, due to the strongly changed interplay of the shift and broadening of the exciton resonance together with the carrier density (see Fig. 8).

Calculating the complex coefficient of reflection with the many-layer model described in Section 3 one has first to determine the real part of the susceptibility. As already described in the last section we have performed a

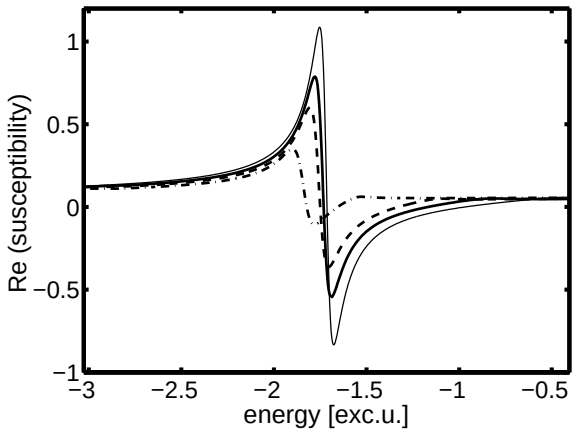

Fig. 10. Real part of the susceptibility for the 19.8 nm quantum well with increasing excitation corresponding to Figure 6.

Kramers-Kronig transformation for the difference between the imaginary parts of the susceptibility for the excited and the non-excited sample and afterwards added the real part for the unexcited sample from the broadened Elliot formula [7]. The behavior of the real part of the susceptibility is similar for all wells and is shown in Figure 10 exemplarily for the 19.9 nm well.

The changes with increasing excitation correspond to that of the imaginary part. In contrast to the well separated exciton resonances in the imaginary parts, the excitonic features in the real parts are much more extended, leading to an overlap of the contributions coming from the different wells and heavy- and light-hole excitons, respectively. Consequently, the exact knowledge of the real part of the susceptibility is absolutely necessary. The good agreement between theory and experiment in Figures 5 and 6 proves the power of our many-body approach.

5 Summary

Summarizing, we have investigated the influence of thermalized non-coherent carriers on the complex coefficient of reflection and the dielectric function of GaAs quantum wells with different well widths. Using the method of spectral interferometry characteristic changes of both the amplitude and the phase of the coefficient of reflection are observed for increasing carrier densities. While the amplitude behaves similar in all wells and will be broadened and smeared out with increasing excitation, the behavior of the phase differs from well to well. On the one hand we find a jump of 2π at the exciton resonance, which is stabilized with increasing excitation, and for other wells a more dispersive behavior, which is as broadened and smeared out as the amplitudes are. The experimental results for the non-excited sample can be described, fitting the exciton parameters and a phenomenological parameter of the effective dimension for the single wells in a broadened Elliot formula. Moreover, we find perfect agreement with a strict microscopic approach based on the Semiconductor Bloch Equations accounting the confinement of carriers in the wells by an expansion with respect to the sub-band wave functions of carriers. In order to describe the carrier-induced changes of the coefficient of reflection we extend the semiconductor Bloch equation incorporating many-body effects which take into account memory effects in the scattering processes between carriers and the polarization induced by the probe pulse. We show, that our theoretical approach is able to describe both spectral properties of the exciton and finally all changes of the complex coefficient of reflection induced by thermalized non-coherent carriers.

We would like to thank D. Reuter and A. Wieck, Ruhr-Universität Bochum, Germany for supplying the sample and the Deutsche Forschungsgemeinschaft for support.

References

1. H. Stolz, *Time-Resolved Light Scattering from Excitons* (Springer, Berlin, 1994)
2. H. Stolz, Ch. Nacke, B. Seifert, M. Seemann, F. Kieseling, Adv. Solid State Phys. **39**, 473 (1999)
3. D.S. Chemla, J.-Y. Bigot, M.-A. Mycek, S. Weiss, W. Schäfer, Phys. Rev. B **50**, 8439 (1994)
4. L. Lepetit, G. Chériaux, M. Joffre, J. Opt. Soc. Am. B **12**, 2467 (1995)
5. J. Tignon, M.V. Marquezini, T. Hasche, D.S. Chemla, IEEE J. Quantum Electronics **25**, 510 (1999)
6. M.V. Marquezini, J. Tignon, T. Hasche, D.S. Chemla, Appl. Phys. Lett. **73**, 2313 (1998)
7. C. Tanguy, P. Lefebvre, H. Mathieu, R.J. Elliot J. Appl. Phys. **82**, 798 (1997)
8. S. Schmitt-Rink, D.S. Chemla, D.A.B. Miller, Phys. Rev. B **32**, 6601 (1985)
9. S. Schmitt-Rink, C. Ell, H. Haug, Phys. Rev. B **33**, 1183 (1986)
10. M.F. Pereira Jr., S.W. Koch, W.W. Chow, J. Opt. Soc. Am. B **10**, 765 (1993)
11. M.F. Pereira, K. Henneberger, Phys. Stat. Sol. (b) **206**, 477 (1998)
12. M.F. Pereira Jr., K. Henneberger, Phys. Rev. B **58**, 2064 (1998)
13. H. Haug, J. Liebler, R. Leonelli, A. Manar, J.B. Grun Phys. Rev. B **38**, 10903 (1988)
14. D. Campi, C. Coriasso, Phys. Rev. B **51**, 10719 (1995)
15. M. Lindberg, S.W. Koch, Phys. Rev. B **38**, 3342 (1988)
16. A. Girndt, F. Jahnke, A. Knorr, S.W. Koch, W.W. Chow, Phys. Stat. Sol. (b) **202**, 725 (1997)
17. F. Jahnke, M. Kira, S.W. Koch, Z. Phys. B **104**, 559 (1997)
18. S. Hughes, A. Knorr, S.W. Koch, R. Binder, R. Indik, J.V. Moloney, Solid State Commun. **100**, 555 (1996)
19. H. Haug, A.P. Jauho, *Quantum Kinetics in Transport and Optics of Semiconductors* (Springer, Berlin Heidelberg, 1996)
20. M. Bonitz, *Quantum Kinetic Theory, Teubner Texte zur Physik* (B.G. Teubner Stuttgart, Leipzig, 1998)
21. W.A. Hügel, M.F. Heinrich, M. Wegener, Q.T. Vu, L. Banyuai, H. Haug, Phys. Rev. Lett. **83**, 3313 (1999)
22. B. Miek, H. Haug, W.A. Hügel, M.F. Heinrich, M. Wegener, Phys. Rev. B **62**, 2686 (2000)

23. Q.T. Vu, H. Haug, W.A. Hügel, S. Chatterjee, M. Wegener Phys. Rev. Lett. **85**, 3508 (2000)
24. J.S. Nägerl, B. Stabenau, G. Böhne, S. Dreher, R.G. Ulbrich, G. Manzke, K. Henneberger, Phys. Rev. B **63**, 235202 (2001)
25. S. Eshlaghi, Ph.D. thesis, Ruhr-Universität Bochum (2000)
26. D.J. Kane, IEEE J. Quantum Electronics **35**, 421 (1999)
27. M.A. Afromowitz Solid State Comm. **15**, 59 (1974)
28. K. Henneberger, H. Güldner, G. Manzke, Q.Y. Peng M.F. Pereira, JR., Adv. Solid State Phys. **38**, 61 (1999) (Vieweg, Wiesbaden, 1999)
29. G. Manzke, Q.Y. Peng, K. Henneberger, U. Neukirch, K. Hauke, K. Wundke, J. Gutowski, D. Hommel, Phys. Rev. Lett. **80**, 4943 (1998)
30. G. Manzke, K. Henneberger, Phys. Stat. Sol. (b) **234**, 233 (2002)
31. R. Binder, A.E. Paul, D. Scott, K. Henneberger, S.W. Koch, Phys. Rev. B **45**, 1107 (1992)
32. Note, to convert the experimental fluences into carrier densities, an additional factor of 2 is required to take into account the smaller spot size of the test pulse